Numerical investigation of the inertial cavitation threshold by dual-frequency excitation in the fluid and tissue

Mingjun Wang[1, 2] ,Yufeng Zhou[1]

1. School of Mechanical and Aerospace Engineering, Nanyang Technological University, 50 Nanyang Ave., Singapore, 639798

2. Motor Group, R&D
ASM Pacific Technology Ltd
3/F, Watson Centre, 16-22 Kung Yip St, Kwai Chung, Hong Kong, PR.China

Abstract

Inertial cavitation thresholds, which are defined as bubble growth by 2-fold from the equilibrium radius, by two types of ultrasonic excitation (at the classical single-frequency mode and dual-frequency mode) were calculated. The effect of the dual-frequency excitation on the inertial cavitation threshold in the different surrounding media (fluid and tissue) was studied, and the paramount parameters (driving frequency, amplitude ratio, phase difference, and frequency ratio) were also optimized to maximize the inertial cavitation. The numerical prediction confirms the previous experimental results that the dual-frequency excitation is capable of reducing the inertial cavitation threshold in comparison to the single-frequency one at the same output power. The dual-frequency excitation at the high frequency (i.e., 3.1+3.5 MHz vs. 1.1+1.3 MHz) is preferred in this study. The simulation results suggest that the same amplitudes of individual components, zero phase difference, and large frequency difference are beneficial for enhancing the bubble cavitation. Overall, this work may provide a theoretical model for further investigation of dual-frequency excitation and guidance of its applications for a better outcome.

Keywords: acoustic cavitation, inertial cavitation threshold, dual-frequency excitation

1. Introduction

Acoustic cavitation induced by ultrasonic irritation, stable and inertial cavitation, is known to play a key role in a wide range of therapeutic ultrasound applications [1, 2]. Bubble oscillation about its equilibrium radius at the low acoustic pressure is termed as stable cavitation whereas inertial cavitation releases high energy, increases the temperature of the vapor to several thousand kelvins, and generates high pressure and/or high-speed jets at the bubble collapse, which may produce mechanical damages to the nearby media [3, 4]. Increasing the driving acoustic pressure could result in the transition from stable cavitation to inertial cavitation. Examples of successful ultrasound therapies utilizing acoustic cavitation include the tissue heating in which stable cavitation causes high shear stress between the bubble and surrounding medium and inertial cavitation produces the broadband noise emission for the substantially promoted and enhanced thermal deposition [5, 6]; histotripsy in which inertial cavitation releases shockwaves capable of destroying cell membranes, mechanically fractionating the soft tissues, and in many cases even completely liquefying them into subcellular components [7, 8]; thrombolysis in which stable cavitation in the vicinity of blood clots promotes the uptake of lytic agent and inertial cavitation produces micro-jet and pitting to directly and mechanically damage the clot's surface [9, 10]; blood-brain barrier (BBB) opening in which stable cavitation temporarily affects the integration of the tight junction and reduces the blood flow. It could be seen that stable cavitation and inertial cavitation function distinctively different in the aforementioned cavitation facilitated therapeutic processes. Therefore, it is of a great concern to determine the threshold pressure for the transition from stable cavitation to inertial cavitation in order to assess the likelihood of different ultrasound-induced bio-effects.

In contrast to the conventional single-frequency acoustic excitation, the dual- or multiple-frequency excitation shows some remarkable merits in sonoluminescence and sonochemistry, such as low cavitation threshold, more chemical activities, and high reaction efficiency, effective elimination of standing wave, and better control over the cavitational activity in the acoustic field in terms of bubble oscillation mode and the spatial distribution [11]. The maximum photocurrent could be boosted up to 300% using double harmonic driving compared with single harmonic driving [12]. In the context of biomedicine, some initial investigations of enhancing the inertial cavitation by the dual-frequency have also been carried out. Dual-frequency excitation in both kHz (525+565 kHz) and MHz (~1.5 MHz) improved the *in vitro* thrombolysis efficiency [13, 14]. Guo et al. [15] showed ~5% to 10% improvement in the temperature elevation in the chicken breast by the dual-frequency excitation. Kuang et al. [16] and He et Al. [17] have demonstrated that using two confocal transducers driven at two neighboring frequencies (1.495+1.505 MHz and 1.563+1.573 MHz) a large lesion could be achieved. Liu et al. [18] and Chen et al. [19] showed that lesions created by the dual-frequency excitation were more uniform and closer to the desired target region. Dual-frequency (500 kHz + 3 MHz) excitation in histotripsy has been shown to precisely tailor the bubble expansion [20, 21]. Sokka et al. [22] have successfully manipulated the cavitation distribution and preferentially lowered the cavitation threshold at the focus by the means of dual-frequency phased array. The first *in vivo* dual-frequency sonodynamic therapy performed on mice showed more effective in terms of suppressing tumor growth and reducing the tumor volumes [23].

The mechanism for the enhancement of bubble cavitation by dual- or multiple-frequency excitation has not been fully understood although some unique characteristics were found in some preliminary investigations. The modeling developed by Zhang et al. [24] shows that bubble

cavitation induced by the dual-frequency excitation has a reduced critical radius for the generation of inertial cavitation comparing with that by the single-frequency one. Acoustical scattering cross section by the dual-frequency excitation displayed more resonances for a much broader range of bubbles [25]. In addition, dual-frequency excitation can lead to a more rapid growth of a wide range of bubbles through the rectified mass diffusion as long as the acoustic pressure is above a certain threshold [26].

So far, plenty of experimental work has confirmed that the dual-frequency excitation could significantly reduce the inertial cavitation threshold [27, 28], but few theoretical studies have been devoted to this subject. Numerical modeling shows promise towards understanding the mechanisms due to its universe applications under various conditions. A theoretical prediction of the inertial cavitation threshold by dual-frequency excitation in the various media, such as fluid (i.e., water and blood) and viscoelastic tissue (i.e., kidney and liver), was studied here, and the paramount parameters that influence the inertial cavitation threshold (i.e., amplitude ratio, phase difference, frequency ratio) were thoroughly investigated in order to optimize the bubble dynamics.

2. Methods

For the single-frequency excitation, the driving signal is described as:

$$P_a = P_A \sin(2\pi f t) \tag{1}$$

where f is the driving frequency and P_A is the acoustic pressure. For the dual-frequency excitation, the driving signal is described as:

$$P_a = P_1 sin(2\pi f_1 t) + P_2 sin(2\pi f_2 t + \varphi) \tag{2}$$

where f_1 and f_2 (usually $f_1 < f_2$) and P_1 and P_2 are the driving frequencies and acoustic pressures of two harmonics, respectively, and φ is the phase difference between them. The common setting is $P_1 = P_2 = P_A/\sqrt{2}$, where the coefficient $1/\sqrt{2}$ is to ensure the same acoustic output power delivered as that of the single-frequency excitation.

Since the bubble behaves differently in various media, two theoretical models are employed to calculate its dynamics in the fluid and tissue. For simplicity, several important assumptions are made [29-31]. 1) The medium is homogeneous and isotropic; 2) The air bubble is always spherical and initially at rest ($\dot{R} = 0$) so that bubble dynamics can be calculated in one-dimensional space; 3) The gas inside the bubble is ideally adiabatic (γ = 1.4); 4) There is no gas or vapor exchange between the gas and the surrounding medium; 5) The pressure inside the bubble is spatially uniform, and the vapor pressure is constant throughout the bubble oscillation.

For the fluid (i.e., water and blood), the Gilmore-Akuliches equation was utilized [32].

$$R\left(1-\frac{U}{C}\right)\frac{dU}{dt}+\frac{3}{2}\left(1-\frac{U}{3C}\right)U^2=\left(1+\frac{U}{C}\right)H+\frac{1}{C}\left(1-\frac{U}{C}\right)R\frac{dH}{dt} \tag{3}$$

where R is the bubble radius, U (= dR/dt) is the velocity at the bubble wall, and C and H are the speed of sound in the liquid at the bubble wall and enthalpy difference between the pressure at the bubble wall $P(R)$ and the pressure at infinity P_∞, respectively, which are given by

$$H = \int_{P_\infty}^{P(R)} \frac{dP}{\rho} \tag{4}$$

$$C = [C_l^2 + (m-1)H]^{1/2} \tag{5}$$

where P is the time-varying pressure, ρ is the medium density, C_l is the infinitesimal speed of sound in the liquid, and m is a constant normally set to 7. The state equation of a compressible fluid and $P(R)$ in relation to the gas pressure inside the bubble of P_g, medium viscosity of μ, and surface tension of σ in the liquid are given by

$$P = A(\rho / \rho_0)^m - B \tag{6}$$

$$P(R) = P_g - \frac{2\sigma}{R} - \frac{4\mu}{R}U \tag{7}$$

where ρ_0 is the equilibrium liquid density, $A = C_l^2\rho/P_0$ and $B = A - 1$ are two constants.

Whereas in the tissue, the bubble dynamics was modeled by the modified Keller-Miksis equation that includes the compressibility and viscoelasticity of the surrounding medium [30].

$$(1-\frac{\dot{R}}{c})R\ddot{R} + \frac{3}{2}(1-\frac{\dot{R}}{3c})\dot{R}^2 = (1+\frac{\dot{R}}{c})[\frac{p_B - p_\infty(t)}{\rho} - \frac{4\mu\dot{R}}{R} - \frac{2S}{\rho R} - E_{NT}] + \frac{R}{\rho c}\frac{d}{dt}(p_a - p_\infty) \tag{8}$$

where c is the constant speed of sound in the medium, and S is the surface tension coefficient. Kelvin–Voigt approach was used to model the viscoelasticity of tissue. Considering the large deformations during the bubble growth, a hyperelastic (Neo-Hookean) constitutive relation was utilized to yield the elastic term [33].

$$E_{NT} = \frac{G}{2}\left[5 - 4\left(\frac{R_0}{R}\right) - \left(\frac{R_0}{R}\right)^4\right] \tag{9}$$

where R_0 is the initial bubble radius, and G is the linear shear modulus.

There are many definitions of the inertial cavitation threshold [31, 34-36]. The maximum bubble expansion to twice of the initial bubble radius is commonly used in the investigation of

cavitation and chosen as the onset of inertial cavitation in this paper. The Gilmore and Keller-Miksis equations were numerically solved using the fifth-order Runge-Kutta-Fehlberg method with a step-size control algorithm in MATLAB (MathWorks, Naticks, MA, USA) with an absolute and relative tolerance of 1e-12 and 1e-7, respectively, to obtain the radius-time profiles with satisfactory precision. The sonication period is 60 μs, which is sufficiently long for bubble dynamics. Throughout this study, the threshold value was determined by varying the acoustic pressure in a step size of 2 kPa for a bubble radius ranging from 0.1 μm to 10 μm. The driving frequencies (f_1 and f_2) were set to 1.1 MHz and 1.3 MHz, 3.1 MHz, and 3.5 MHz, which are within the -6 dB bandwidth of a commercial HIFU transducer (H102, Sonic Concepts, Woodinville, WA, USA) at its fundamental and third harmonic. Water, blood, kidney, and liver are commonly used for the study of sonochemistry reaction, thrombolysis, blood-brain barrier opening, and ultrasound-induced biological effects, respectively, and their physical parameters are listed in Table 1 [31, 37]. Vapor pressure in the tissue and ambient pressure were assumed to be 6 kPa and 101.3 kPa, respectively.

3. Results

3.1. Bubble dynamics

With the introduction of another acoustic wave in the dual-frequency excitation, the driving signal is in a beat mode with repetitive construction and destruction. The representative bubble dynamics driven by the single- and dual-frequency excitation (1.1+1.3 MHz and 3.1+3.5 MHz) are shown in Figs. 1 and 2, respectively. Initial bubble size was set to 1 μm while the acoustic pressure to 5 bars. It is found that the bubble dynamics relies on both the surrounding medium and the excitation source. The dual-frequency excitation at the high frequency (3.1+3.5 MHz) has smaller bubble radius than that at the low frequency (1.1+1.3 MHz). The damping time for a bubble in the water and blood was around 3 cycles for the single-frequency excitation. However, the bubble got a steady oscillation immediately for the dual-frequency excitation. The viscoelasticity of tissue restricts the bubble oscillation, reducing the amplitude and nonlinearity [31]. Subsequently, the bubble oscillation in the tissue was immediately stabilized regardless of the excitation conditions. Furthermore, the bubble expansion by the dual-frequency excitation is clearly larger than that of the single-frequency one, particularly in the tissue and at the high frequency. The maximum bubble radius under the dual-frequency excitation (3.1+3.5 MHz) is 1.22 fold of 3.1 MHz-excitation in the liver, but only 1.1 fold in the water.

The bubble dynamics in the tissue under the dual-frequency excitation also shows some unique characteristics in comparison to that in the fluid. The bubble oscillation exhibits not only larger maximum expansion but also smaller minimum compression, implying a higher internal temperature. In addition, the bubble collapse time, t_c, the interval time between the bubble reaching its maximum size and becoming less than 1% of the initial size [11], is not severely altered by the dual-frequency excitation. The increased maximum bubble radius, reduced

minimum bubble radius, and the unaffected bubble collapse time (characterized by R_{max}^3/t_c and R_{max}/R_{min}) lead to the enhanced strength and temperature of bubble collapse, which is particularly preferred for the induced bio-effects [38, 39]. The simulation results are summarized in Tables 2 and 3. The increased viscoelasticity of surrounding medium (tissue vs. fluid) reduces the violence of bubble growth and collapse significantly. The value of R_{max}/R_{min} in the water under the ultrasound exposure at the frequency of 3.1 MHz, 3.5 MHz, and 3.1+3.5MHz was 23.92, 19.47, and 28.05, respectively; whereas the corresponding values in the liver are 3.77, 3.37, and 7.72, respectively. The enhancement of dual-frequency excitation to the single-frequency one in the liver is about 2.3 fold, but only 1.4 fold in the water.

3.2. Inertial cavitation threshold

The inertial cavitation thresholds using the single- and dual-frequency excitations were calculated in all the aforementioned media with the bubble radius ranging from 0.1 μm to 10 μm in a step size of 0.1 μm and illustrated in Figure 3. It is found that the inertial cavitation threshold initially drops to the global minimum and then gradually increases with the initial bubble radius. The dual-frequency excitation could significantly lower the inertial cavitation threshold, particularly in the blood and water. Both the high driving frequency and viscoelasticity lead to an increase of the threshold. The inertia of the surrounding medium suppresses the bubble collapse during the half-cycle of the compressive wave, and then bubble continues to grow during the following half-cycle of the tensile wave, hence leading to a higher cavitation threshold [40]. However, the inertial cavitation thresholds in the water and blood have small variations comparing with those in the kidney and liver, particularly for the large initial bubble radii at the high frequency. This occurrence may be due to the onset of chaotic oscillations, where bubble collapses at irregular intervals [41].

The optimal bubble size and the corresponding inertial cavitation threshold are summarized in Table 4. It could be seen that the dual-frequency excitation does not significantly change the optimal bubble size but only reduce the inertial cavitation threshold. The optimal bubble size is a function of the driving frequency and acoustic pressure given by [42]:

$$R(p,f) = \frac{1}{\sqrt{G(f) + K \cdot p^2}} \tag{10}$$

where *G(f)* is a function of frequency independent of the acoustic pressure, *K* is an unknown constant, and *p* is the acoustic pressure. The linear resonant frequency for a specific bubble size in the fluid [43] and tissue [33, 44] can be described by the following equations, respectively.

$$f = \frac{1}{2\pi R_0\sqrt{\rho}}\sqrt{3\gamma\left(p_0 - p_v + \frac{2S}{R_0}\right) + p_v - \frac{2S}{R_0} - \frac{4\mu^2}{\rho R_0^2}} \tag{11}$$

$$f = \frac{1}{2\pi R_0\sqrt{\rho}}\sqrt{3\gamma(p_0 - p_v) + (3\gamma - 1)\frac{2S}{R_0} - \frac{8\mu^2}{\rho R_0^2} + 4G} \tag{12}$$

The resonant structure is related to the (sub) fractional-order subharmonic resonance minima as described previously [45] and shown by arrows in Fig. 3. Another noticeable trend in the threshold is the shift of local resonance minima by the dual-frequency excitation. Because of the interference of individual components, bubble oscillation by the dual-frequency excitation shows a combination resonance and simultaneous resonance and hence is initially assumed to have more local minima [46]. Nevertheless, our calculation results have a much smaller amount of local minima for the dual-frequency excitation, 4 local minima for the dual-frequency excitation vs. 7 or 8 for the single-frequency excitation in Fig. 3b, which further testifies the previous conclusion that the dual-frequency excitation may lead to a stabilized bubble oscillation [47]. Furthermore, it is worth noticing that the inertial cavitation threshold by the dual-frequency excitation at the high

frequency is not only lower than that of the individual component (3.1 MHz and 3.5 MHz) but also lower than that of 1.1 MHz and 1.3 MHz when the bubble size is no larger than about 0.5 μm, which is likely related to the bubble resonance size (see the inset plot in Fig.3). It is well known that the resonant bubble size is inversely proportional to the driving frequency and the growth of small bubble is highly sensitive around the resonance regime so that even a small frequency change results in a large variation of resonant bubble radius. Therefore, bubble oscillation is more significant with more occurrence of bubble collapse by the dual-frequency excitation at the high frequency because of broad frequency span range covering more resonant bubble sizes. Since inertial cavitation threshold is strongly dependent on the initial bubble size, the validity of this study essentially relies on the pre-existence of stabilized small bubble nuclei. It has been reported that the radius of cavitation nuclei in the water is in the order of 1 μm or less and the distribution density decreases exponentially with the radius [48, 49]. However, the nuclei radii *in vivo* were estimated to be less than 0.3 μm [50, 51]. Therefore, the bubble size in the range of 0.1-10 μm used here is close to the real cases. In summary, the dual-frequency excitation at the high frequency is preferable for the small bubbles in the tissue.

3.3. Parameter optimization

In this sub-section, the influences of the paramount parameters (i.e. amplitude ratio, phase difference, and frequency ratio) of the dual-frequency excitation on the inertial cavitation threshold were numerically investigated. Each individual parameter was varied by keeping the rest constant.

3.3.1. Amplitude ratio

For the convenient discussion, the ratio of two acoustic pressure amplitudes is defined as $N_p = P_2/P_1$ and was varied from 0.1 to 10 in a step size of 0.1, implying the gradual shift of

energy from the low-frequency component to the high-frequency one. The frequencies were kept as 1.1+1.3MHz and 3.1+3.5 MHz, and the phase difference was set to zero. Generally, the influence of the amplitude ratio is more significant for a large bubble (see Fig. 4 and Fig. 5). Small bubbles are resistant to the change of amplitude ratio, which may be due to the large surface tension [52]. The inertial cavitation threshold with the amplitude ratio of Np = 0.1, 0.5, 1.0, 2.0, and 5.0 was compared in Fig. 6. Because of the onset of chaotic oscillation, the inertial cavitation threshold varies significantly over the range of bubble radius investigated, and the optimal amplitude ratio depends on both the bubble radius and the surrounding medium. The inertial cavitation threshold at Np = 1 is found always lower than the other ratios under all simulation conditions. Finally, the dual-frequency excitation at the high frequency favors a reduced threshold, particularly in the fluid. Overall, the optimal amplitude ratio is suggested to be close to 1 for all bubble sizes investigated.

3.3.2. Phase difference

The phase difference between two individual components affects the acoustic pressure distribution, the energy dissipation, the radical production, and even the onset of chaotic oscillation [47, 53]. Here the phase difference increased from 0 to 2π in a step of π/18 (10°), and its influence on the inertial cavitation threshold is shown in Fig. 7 and Fig. 8. The inertial cavitation threshold is the lowest when the two components are in phase (φ = 0 or 2π), but the highest for out of phase (φ = π). Furthermore, a large bubble is more sensitive to the phase difference, which is more apparent in the fluid at the high frequency. Few variations of the threshold are found for bubbles in the tissue at the low-frequency excitation (see Fig. 9c and 9d). The inertial cavitation threshold in the fluid is initially not affected much by the phase difference (see Fig. 9). But the discrepancy becomes significant when the initial bubble radius is larger than 2.5 μm by the

excitation of 3.1+3.5 MHz and 6.8 μm by the excitation of 1.1+1.3 MHz in the water, and the corresponding values are 1.0 μm and 6.2 μm in the blood, respectively. The critical bubble radius for the significant impact of the phase difference at the high frequency is 5.8 μm and 5 μm for the liver and the kidney, respectively. However, the phase difference seems to be more insensitive to the bubble radius at the low frequency, which may be due to the reduced nonlinearity of bubble oscillation as a consequence of the long rarefaction duration [54].

3.3.3. Frequency ratio

The frequency ratio is defined as $N_f = f_1/f_2$ and varies from 0.1 to 10 in a step size of 0.1 (setting $\varphi = 0$, $Np = 1$, and $f_2 = 1.1$ MHz or 3.1MHz). The influences of the frequency ratio are shown in Figs. 10-12. The inertial cavitation threshold first increases rapidly with the frequency ratio and then remains quite stable. Large initial bubbles are insensitive to the change of frequency ratio, which is contrary to the cases of the amplitude ratio and phase difference. The fluctuation of the inertial cavitation threshold at the high frequency is smooth and small, but large and sharp at the low frequency, particularly in the water and blood (see Fig. 12). The larger the frequency difference, the lower of the cavitation threshold. Overall, the results suggest that large frequency difference is favorable for the dual-frequency excitation. However, the practice is usually limited by the bandwidth of a single transducer; otherwise, two or more separated transducers are required.

4. Discussion

In this study, inertial cavitation threshold using the dual-frequency excitation in the fluid and tissue was investigated numerically and compared with that using the single-frequency one, and paramount parameters were optimized. The bubble growth through the rectified mass diffusion by the dual-frequency excitation is so fast that the final equilibrium bubble radius becomes larger [26]. However, the models used here did not account for the gas diffusion across the bubble wall. Such an omission is not critical because the inertial cavities are not likely to survive more than one or two cycles of excitation. Our simulation involved in the mass transfer shows that the difference of maximum bubble radius is less than 1% (data not included), but the computation time is 10 times longer. Under the assumption of the adiabatic process, heat transfer was also neglected. To include its influence, the value of polytropic exponent can simply be changed from 1.4 to 1.0 at the maximum bubble expansion, which means the isothermal process. It has been shown that the adiabatic assumption underestimated the maximum bubble radius while the isothermal assumption overestimated it [55]. The error between these two assumptions was approximately 10% and acceptable in the simulation. The temperature variation also plays a significant role in the inertial cavitation threshold. Higher ambient temperature leads to a lower cavitation threshold in the fluid, but a slightly higher one in the tissue [40]. This study did not consider this effect because the inertial cavitation occurs in such a short time that the bubble does not have sufficient time for the thermal response. Although multiple-frequency excitations were able to enhance the temperature elevation in the tissue ablation because of the enhanced inertial cavitation, the temperature elevation in the pulsed ultrasound application, such as sonothrombolysis, is insignificant [56]. Furthermore, dual-frequency excitation has less acoustic absorption than the single-frequency mode at the same power because of the reduced waveform distortion [57].

The interaction between bubbles also has a great impact on their dynamics. When numerous bubbles with different radii are presented, the radiation pressure generated by the bubble oscillation attracts or repulses the neighboring bubbles mutually. The velocity and amplitude of the acoustic waves will be modified when traveling through the bubbly liquids with much higher acoustic attenuation and scattering [58, 59]. It has been shown that the inertial cavitation threshold of an encapsulated microbubble increases with its concentration [60]. In addition, the sign and strength of the Bjerknes force between two bubbles under the dual-frequency excitation showed a complicated pattern [20]. Therefore, the determination of inertial cavitation at the presence of bubble cloud is quite challenging and needs continuous investigations.

Nonlinear distortion in the acoustic wave propagation was not taken into account in this study, which limits the accuracy of the prediction, especially for the applications at the high acoustic intensity [61]. Due to the nonlinear nature of bubble dynamics, waveform distortion or the formation of shock front is likely to have a great influence. It has been shown that higher-order harmonics introduced in the distorted waveform have little effect on the occurrence of inertial cavitation because bubbles respond well below their resonant frequencies and the fundamental harmonic is suggested to be the major contributor for the inertial cavitation [55, 62]. Nevertheless, the recent study revealed that the maximum bubble size undergoing inertial cavitation was reduced with the consideration of the nonlinear waveform distortion [63], which implies that our simulation utilizing an ideal sinusoidal wave may overestimate the inertial cavitation threshold. However, the discrepancy is less at the dual-frequency excitation because of less waveform distortion. Therefore, the predicted inertial cavitation threshold of the dual-frequency excitation is more reliable than that of the single-frequency one, especially at the low frequency and acoustic pressure.

Although the simulation has confirmed the experimental observation that dual frequency can reduce the inertial cavitation threshold, the underlying mechanisms are complex and still not very clear now. So far, several possibilities have been presented. Firstly, the dual-frequency irritation can produce more bubble nucleation as the result of the low-frequency stimulation and the intensified Bjerknes force[20]. Secondly, bubble oscillation by the dual-frequency excitation shows a combination resonance and simultaneous resonance, which could cause cavitation over a wider range of bubble radii[46]. Lastly, the increased peak negative pressure by the dual-frequency excitation diminishes the cavitation threshold and increases the number of bubbles. This quasi-static pressure contributes to an increase of the collapse rate during the positive pressure [64, 65].

5. Conclusion

In this study, the effect of dual-frequency excitation on the inertial cavitation threshold was calculated in the both fluid and tissue and compared with the single-frequency excitation. It is found that the induction of another acoustic component into the excitation can substantially reduce the inertial cavitation threshold. The effect of paramount parameters (amplitude ratio, phase difference, and frequency ratio) of the dual-frequency excitation on the inertial cavitation threshold was also studied to optimize the outcome. It is shown that the amplitude ratio of 1 (same amplitude for each individual component), the phase difference of 0 or 2π (in phase), and the large frequency difference would achieve the best performance, the low inertial cavitation threshold. Experimental measurement is required to confirm our conclusions. Further investigation, such as increasing the acoustic intensity, would extend our work for a wide range of practical applications.

References

1. Brennen, C.E., *Cavitation in medicine.* Interface focus, 2015. **5**(5): p. 20150022.
2. Noltingk, B.E. and E.A. Neppiras, *Cavitation produced by ultrasonics.* Proceedings of the Physical Society. Section B, 1950. **63**(9): p. 674.
3. Tung, Y.S., et al., *In vivo transcranial cavitation threshold detection during ultrasound-induced blood-brain barrier opening in mice.* Phys Med Biol, 2010. **55**(20): p. 6141-55.
4. Blake, J.R., D.M. Leppinen, and Q. Wang, *Cavitation and bubble dynamics: the Kelvin impulse and its applications.* Interface focus, 2015. **5**(5): p. 20150017.
5. Coussios, C.C. and R.A. Roy, *Applications of Acoustics and Cavitation to Noninvasive Therapy and Drug Delivery.* Annual Review of Fluid Mechanics, 2008. **40**(1): p. 395-420.
6. Coussios, C.C., et al., *Role of acoustic cavitation in the delivery and monitoring of cancer treatment by high-intensity focused ultrasound (HIFU).* International Journal of Hyperthermia, 2007. **23**(2): p. 105-120.
7. Xu, Z., et al., *Controlled ultrasound tissue erosion.* Ultrasonics, Ferroelectrics, and Frequency Control, IEEE Transactions on, 2004. **51**(6): p. 726-736.
8. Khokhlova, T.D., et al., *Controlled tissue emulsification produced by high intensity focused ultrasound shock waves and millisecond boiling.* J Acoust Soc Am, 2011. **130**(5): p. 3498-510.
9. Datta, S., et al., *Correlation of cavitation with ultrasound enhancement of thrombolysis.* Ultrasound in medicine & biology, 2006. **32**(8): p. 1257-1267.
10. Petit, B., et al., *Sonothrombolysis: the contribution of stable and inertial cavitation to clot lysis.* Ultrasound Med Biol, 2015. **41**(5): p. 1402-10.
11. Tatake, P.A. and A.B. Pandit, *Modelling and experimental investigation into cavity dynamics and cavitational yield: influence of dual frequency ultrasound sources.* Chemical Engineering Science, 2002. **57**(22): p. 4987-4995.
12. Holzfuss, J., M. Rüggeberg, and R. Mettin, *Boosting sonoluminescence.* Physical review letters, 1998. **81**(9): p. 1961.
13. Saletes, I., et al., *In vitro demonstration of focused ultrasound thrombolysis using bifrequency excitation.* BioMed research international, 2014. **2014**.
14. Suo, D., et al., *Thrombolysis using multi-frequency high intensity focused ultrasound at MHz range: an in vitro study.* Physics in medicine and biology, 2015. **60**(18): p. 7403.
15. Guo, S., Y. Jing, and X. Jiang, *Temperature rise in tissue ablation using multi-frequency ultrasound.* Ultrasonics, Ferroelectrics, and Frequency Control, IEEE Transactions on, 2013. **60**(8): p. 1699-1707.
16. Kuang, S.L., et al., *Confocal dual-frequency enhances the damaging effect of high-intensity focused ultrasound in tissue-mimicking phantom.* Minim Invasive Ther Allied Technol, 2008. **17**(5): p. 285-91.
17. He, P.Z., et al., *The affection on the tissue lesions of difference frequency in dual-frequency high-intensity focused ultrasound (HIFU).* Ultrason Sonochem, 2006. **13**(4): p. 339-44.
18. Liu, H.L., et al., *Cavitation-enhanced ultrasound thermal therapy by combined low- and high-frequency ultrasound exposure.* Ultrasound Med Biol, 2006. **32**(5): p. 759-67.
19. Chen, W.S., et al., *Reducing lesion aberration by dual-frequency focused ultrasound ablations.* Int J Hyperthermia, 2011. **27**(7): p. 637-47.
20. Zhang, Y., Y. Zhang, and S. Li, *The secondary Bjerknes force between two gas bubbles under dual-frequency acoustic excitation.* Ultrasonics Sonochemistry, 2016. **29**: p. 129-145.
21. Vlaisavljevich, E., et al., *Effects of tissue stiffness, ultrasound frequency, and pressure on histotripsy-induced cavitation bubble behavior.* Phys Med Biol, 2015. **60**(6): p. 2271-92.
22. Sokka, S.D., T.P. Gauthier, and K. Hynynen, *Theoretical and experimental validation of a dual-frequency excitation method for spatial control of cavitation.* Phys Med Biol, 2005. **50**(9): p. 2167-79.
23. Barati, A.H., et al., *Treatment of murine tumors using dual-frequency ultrasound in an experimental in vivo model.* Ultrasound Med Biol, 2009. **35**(5): p. 756-63.
24. Zhang, Y., et al., *Instability of interfaces of gas bubbles in liquids under acoustic excitation with dual frequency.* Ultrason Sonochem, 2015. **23**: p. 16-20.
25. Zhang, Y. and S. Li, *Acoustical scattering cross section of gas bubbles under dual-frequency acoustic excitation.* Ultrason Sonochem, 2015. **26**: p. 437-44.
26. Zhang, Y., *Rectified mass diffusion of gas bubbles in liquids under acoustic field with dual frequencies.* International Communications in Heat and Mass Transfer, 2012. **39**(10): p. 1496-1499.
27. Gilles, B., et al., *Reduction of ultrasound inertial cavitation threshold using bifrequency excitation.* Applied Physics Letters, 2006. **89**(9): p. 094106.

28. Saletes, I., B. Gilles, and J.C. Bera, *Promoting inertial cavitation by nonlinear frequency mixing in a bifrequency focused ultrasound beam.* Ultrasonics, 2011. **51**(1): p. 94-101.
29. Coussios, C., et al., *Role of acoustic cavitation in the delivery and monitoring of cancer treatment by high-intensity focused ultrasound (HIFU).* International Journal of Hyperthermia, 2007. **23**(2): p. 105-120.
30. Yang, X. and C.C. Church, *A model for the dynamics of gas bubbles in soft tissue.* The Journal of the Acoustical Society of America, 2005. **118**(6): p. 3595.
31. Yang, X. and C.C. Church, *Nonlinear dynamics of gas bubbles in viscoelastic media.* Acoustics Research Letters Online, 2005. **6**(3): p. 151-156.
32. Zhu, S. and P. Zhong, *Shock wave–inertial microbubble interaction: A theoretical study based on the Gilmore formulation for bubble dynamics.* The Journal of the Acoustical Society of America, 1999. **106**(5): p. 3024.
33. Gaudron, R., M.T. Warnez, and E. Johnsen, *Bubble dynamics in a viscoelastic medium with nonlinear elasticity.* Journal of Fluid Mechanics, 2015. **766**: p. 54-75.
34. Church, C.C., *Frequency, pulse length, and the mechanical index.* Acoustics Research Letters Online, 2005. **6**(3): p. 162-168.
35. Church, C.C., *A Theoretical Study of Gas Bubble Dynamics in Tissue.* 2006. **838**: p. 217-224.
36. Moholkar, V.S., S. Rekveld, and M.M. Warmoeskerken, *Modeling of the acoustic pressure fields and the distribution of the cavitation phenomena in a dual frequency sonic processor.* Ultrasonics, 2000. **38**(1): p. 666-670.
37. Church, C.C., C. Labuda, and K. Nightingale, *A theoretical study of inertial cavitation from acoustic radiation force impulse imaging and implications for the mechanical index.* Ultrasound Med Biol, 2015. **41**(2): p. 472-85.
38. Kanthale, P.M., et al., *Experimental and theoretical investigations on sonoluminescence under dual frequency conditions.* Ultrason Sonochem, 2008. **15**(4): p. 629-35.
39. Kanthale, P.M., P.R. Gogate, and A.B. Pandit, *Modeling aspects of dual frequency sonochemical reactors.* Chemical Engineering Journal, 2007. **127**(1-3): p. 71-79.
40. Webb, I.R., S.J. Payne, and C.C. Coussios, *The effect of temperature and viscoelasticity on cavitation dynamics during ultrasonic ablation.* J Acoust Soc Am, 2011. **130**(5): p. 3458-66.
41. Zhang, Y., *Chaotic oscillations of gas bubbles under dual-frequency acoustic excitation.* Ultrasonics Sonochemistry, 2017.
42. Carvell, K.J. and T.A. Bigelow, *Dependence of optimal seed bubble size on pressure amplitude at therapeutic pressure levels.* Ultrasonics, 2011. **51**(2): p. 115-22.
43. Lauterborn, W. and T. Kurz, *Physics of bubble oscillations.* Reports on Progress in Physics, 2010. **73**(10): p. 106501.
44. Khismatullin, D.B., *Resonance frequency of microbubbles: Effect of viscosity.* The Journal of the Acoustical Society of America, 2004. **116**(3): p. 1463.
45. Flynn, H.G. and C.C. Church, *Transient pulsations of small gas bubbles in water.* The Journal of the Acoustical Society of America, 1988. **84**(3): p. 985-998.
46. Zhang, Y., Y. Zhang, and S. Li, *Combination and simultaneous resonances of gas bubbles oscillating in liquids under dual-frequency acoustic excitation.* Ultrason Sonochem, 2017. **35**(Pt A): p. 431-439.
47. Behnia, S., et al., *Suppressing chaotic oscillations of a spherical cavitation bubble through applying a periodic perturbation.* Ultrason Sonochem, 2009. **16**(4): p. 502-11.
48. Yount, D., E. Gillary, and D. Hoffman, *A microscopic investigation of bubble formation nuclei.* The Journal of the Acoustical Society of America, 1984. **76**(5): p. 1511-1521.
49. Blatteau, J.-E., et al., *Gas nuclei, their origin, and their role in bubble formation.* Aviation, space, and environmental medicine, 2006. **77**(10): p. 1068-1076 %@ 0095-6562.
50. Gateau, J., et al., *Statistics of acoustically induced bubble-nucleation events in in vitro blood: a feasibility study.* Ultrasound in medicine & biology, 2013. **39**(10): p. 1812-1825.
51. Gateau, J., et al., *In vivo bubble nucleation probability in sheep brain tissue.* Phys Med Biol, 2011. **56**(22): p. 7001-15.
52. Leighton, T., *The acoustic bubble*. 2012: Academic press.
53. Moholkar, V.S., *Mechanistic optimization of a dual frequency sonochemical reactor.* Chemical Engineering Science, 2009. **64**(24): p. 5255-5267.
54. Sadighi-Bonabi, R., F. Alijan Farzad Lahiji, and F. Razeghi, *The effect of viscosity, applied frequency and driven pressure on the laser induced bubble luminescence in water–sulfuric acid mixtures.* Physics Letters A, 2016. **380**(27-28): p. 2219-2226.

55. Aymé, E.J. and E.L. Carstensen, *Cavitation induced by asymmetric distorted pulses of ultrasound: Theoretical predictions.* Ultrasonics, Ferroelectrics, and Frequency Control, IEEE Transactions on, 1989. **36**(1): p. 32-40 %@ 0885-3010.
56. Saletes, I., et al., *In vitro demonstration of focused ultrasound thrombolysis using bifrequency excitation.* Biomed Res Int, 2014. **2014**: p. 518787.
57. Sijia, G., J. Yun, and J. Xiaoning, *Temperature rise in tissue ablation using multi-frequency ultrasound.* IEEE Trans Ultrason Ferroelectr Freq Control, 2013. **60**(8): p. 1699-707.
58. Vanhille, C. and C. Campos-Pozuelo, *Nonlinear ultrasonic propagation in bubbly liquids: a numerical model.* Ultrasound in medicine & biology, 2008. **34**(5): p. 792-808.
59. Zhang, Y. and X. Du, *Influences of non-uniform pressure field outside bubbles on the propagation of acoustic waves in dilute bubbly liquids.* Ultrasonics sonochemistry, 2015. **26**: p. 119-127.
60. Yasui, K., et al., *Influence of the bubble-bubble interaction on destruction of encapsulated microbubbles under ultrasound.* J Acoust Soc Am, 2009. **126**(3): p. 973-82.
61. Wang, M. and Y. Zhou, *Simulation of non-linear acoustic field and thermal pattern of phased-array high-intensity focused ultrasound (HIFU).* International Journal of Hyperthermia, 2016: p. 1-14.
62. Aymé, E.J. and E.L. Carstensen, *Cavitation induced by asymmetric, distorted pulses of ultrasound: A biological test.* Ultrasound in medicine & biology, 1989. **15**(1): p. 61-66.
63. Sinden, D., E. Stride, and N. Saffari. *The effects of nonlinear wave propagation on the stability of inertial cavitation*. in *Journal of Physics: Conference Series*. 2009. IOP Publishing.
64. Feng, R., et al., *Enhancement of ultrasonic cavitation yield by multi-frequency sonication.* Ultrasonics sonochemistry, 2002. **9**(5): p. 231-236.
65. Barati, A.H., et al., *Effect of exposure parameters on cavitation induced by low-level dual-frequency ultrasound.* Ultrason Sonochem, 2007. **14**(6): p. 783-9.

Figure Legends

Figure 1. The instantaneous dynamics of a 1 μm bubble driven by the single- (1.1 MHz and 1.3 MHz) and dual-frequency (1.1+1.3 MHz) at the acoustic pressure of 5 bars in the a) water, b) blood, c) kidney, and d) liver.

Figure 2. The instantaneous dynamics of a 1 μm bubble driven by the single- (3.1 MHz and 3.5 MHz) and dual-frequency excitation (3.1+3.5 MHz) at the acoustic pressure of 5 bars in the a) water, b) blood, c) kidney, and d) liver.

Figure 3. The predicted inertial cavitation threshold (MPa) by the single- (1.1 MHz, 1.3 MHz, 3.1 MHz, and 3.5 MHz) and dual-frequency excitations (1.1+1.3 MHz and 3.1+3.5 MHz) for bubble ranging from 0.1 μm to 10 μm in the a) water, b) blood, c) kidney, and d) liver. The inset plots show the results of bubble ranged from 0.1μm to 1μm.

Figure 4. The inertial cavitation threshold (MPa) at the excitation of 1.1+1.3 MHz as a function of bubble size ranging from 0.1 μm to 10 μm and the amplitude ratio from 0.1 to 10 in a step size of 0.1 in the a) water, b) blood, c) kidney, and d) liver.

Figure 5. The inertial cavitation threshold (MPa) at the excitation of 3.1+3.5MHz as a function of bubble size ranging from 0.1 μm to 10 μm and the amplitude ratio from 0.1 to 10 in a step size of 0.1 in the a) water, b) blood, c) kidney, and d) liver.

Figure 6. The dependence of inertial cavitation threshold (MPa) on the bubble ranging from 0.1 μm to 10 μm at the amplitude ratio of 0.1, 0.5, 1, 2, and 5 driven by the excitations of a) 1.1+1.3 MHz and b) 3.1+3.5 MHz in the water, blood, kidney, and liver (from left to right). The inset plot compares the results of bubble ranging from 0.1μm to 1μm.

Figure 7. The inertial cavitation threshold (MPa) at the excitation of 3.1+3.5 MHz as a function of bubble size ranging from 0.1 μm to 10 μm and the phase difference from 0 to 2π in a step size of π/18 in the a) water, b) blood, c) kidney, and d) liver.

Figure 8. The inertial cavitation threshold (MPa) at the excitation of 1.1+1.3 MHz as a function of bubble size ranging from 0.1 μm to 10 μm and the phase difference from 0 to 2π in a step size of π/18 in the a) water, b) blood, c) kidney, and d) liver.

Figure 9. The inertial cavitation threshold (MPa) of bubble ranging from 0.1 μm to 10 μm at the phase difference of 0, π/2, and π by the excitations of 1.1+1.3 MHz and 3.1+3.5 MHz in the a) water, b) blood, c) kidney, and d) liver.

Figure 10. The inertial cavitation threshold (MPa) by the low dual-frequency excitation (f_2 = 1.1 MHz) as a function of bubble ranging from 0.1 μm to 10 μm and the frequency ratio from 0.1 to 10 in a step size of 0.1 in the a) water, b) blood, c) kidney, and d) liver.

Figure 11. The inertial cavitation threshold (MPa) by the high dual-frequency excitation (f_2 = 3.1 MHz) as a function of bubble ranging from 0.1 μm to 10 μm and the frequency ratio from 0.1 to 10 in a step size of 0.1 in the a) water, b) blood, c) kidney, and d) liver.

Figure 12. The inertial cavitation threshold of the bubble ranging from 0.1 μm to 10 μm at the frequency ratio of 0.1, 0.5, 1.0, 2.0, 5.0, and 10.0 driven by a) low dual-frequency excitation (f_2 = 1.1 MHz) and b) high dual-frequency excitation (f_2 = 3.1 MHz) in the water, blood, kidney and liver (from left to right).

Table

Table 1. Material properties

Material	Sound speed (m/s)	Density (kg/m^3)	Surface tension (mN/m)	Viscosity (mPa·s)	Rigidity (MPa)
Water	1500	1000	68	1.0	0.00
Blood	1570	1050	56	5.0	0.00
Kidney	1561	1100	56	5.0	0.18
Liver	1549	1100	56	9.0	0.04

Table 2. Comparison of the bubble dynamics in water and blood

Material	water					blood				
Frequency (MHz)	R_{max} (μm)	R_{min} (μm)	R_{max}/R_{min}	t_c (μs)	R_{max}^3/t_c	R_{max} (μm)	R_{min} (μm)	R_{max}/R_{min}	t_c (μs)	R_{max}^3/t_c
3.1	3.9996	0.1672	23.92	0.306	209.09	2.8126	0.2678	10.50	0.123	180.89
3.5	3.6892	0.1895	19.47	0.278	180.61	2.8742	0.2675	10.74	0.111	213.91
3.1+3.5	4.3679	0.1557	28.05	0.358	232.77	3.2586	0.2183	14.93	0.125	276.81
1.1	8.2643	0.0657	125.79	0.327	1726.12	5.4786	0.0887	61.77	0.219	750.87
1.3	7.1055	0.0762	93.25	0.289	1241.33	4.6883	0.1086	43.17	0.186	554.03
1.1+1.3	9.2253	0.0678	136.07	0.386	2032.96	7.0516	0.0834	84.55	0.26	1348.62

Table 3. Comparison of the bubble dynamics in the kidney and liver

Material	kidney					liver				
Frequency (MHz)	R_{max} (μm)	R_{min} (μm)	R_{max}/R_{min}	t_c (μs)	R_{max}^3/t_c	R_{max} (μm)	R_{min} (μm)	R_{max}/R_{min}	t_c (μs)	R_{max}^3/t_c
3.1	1.6611	0.4409	3.77	0.078	58.76	1.6147	0.5302	3.05	0.1	42.10
3.5	1.569	0.4658	3.37	0.073	52.91	1.5391	0.5451	2.82	0.084	43.40
3.1+3.5	2.0212	0.2617	7.72	0.073	113.11	1.9835	0.3875	5.12	0.082	95.17
1.1	2.2224	0.4802	4.63	0.133	82.53	3.0928	0.2737	11.30	0.161	183.75
1.3	2.0866	0.4168	5.01	0.122	74.47	2.6916	0.3386	7.95	0.143	136.36
1.1+1.3	3.7296	0.1322	28.21	0.14	370.56	4.5703	0.1548	29.52	0.172	555.02

Table 4. Comparison of the optimal seed bubble size and the corresponding inertial cavitation threshold

Material	Water		Blood		Kidney		Liver	
Frequency (MHz)	Bubble size (μm)	Pressure (MPa)	Bubble size (μm)	Pressure (MPa)	Bubble size (μm)	Pressure (MPa)	Bubble size (μm)	Pressure (MPa)
3.1	1.15	0.0970	1.04	0.3080	1.62	0.4394	1.34	0.6110
3.5	1.04	0.1050	0.97	0.3383	1.46	0.4848	1.23	0.6918
3.1+3.5	1.13	0.0959	1.07	0.2323	1.62	0.3484	1.32	0.4747
1.1	2.83	0.0505	2.54	0.1263	4.20	0.2020	3.12	0.2475
1.3	2.46	0.0505	2.18	0.1465	3.56	0.2273	2.76	0.2828
1.1+1.3	2.63	0.0454	2.51	0.1111	4.04	0.1919	3.13	0.2071

Figure

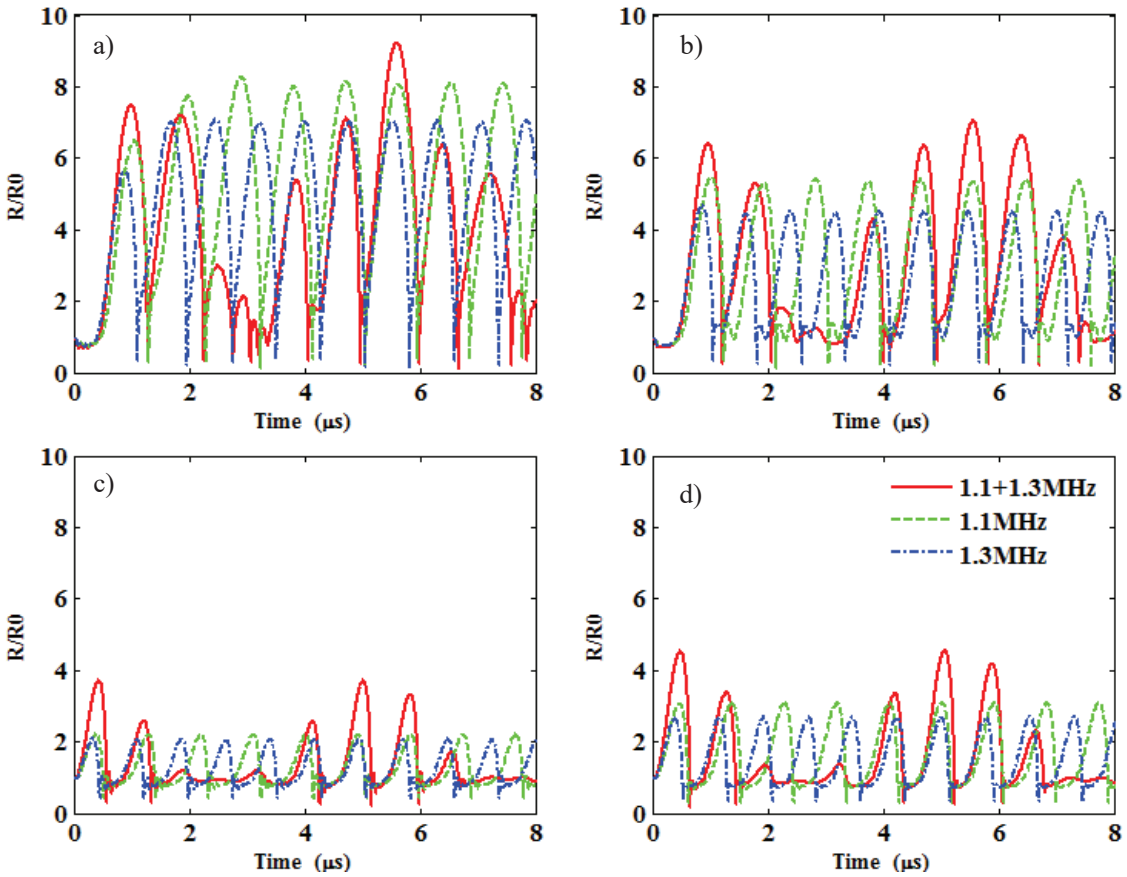

Figure 1

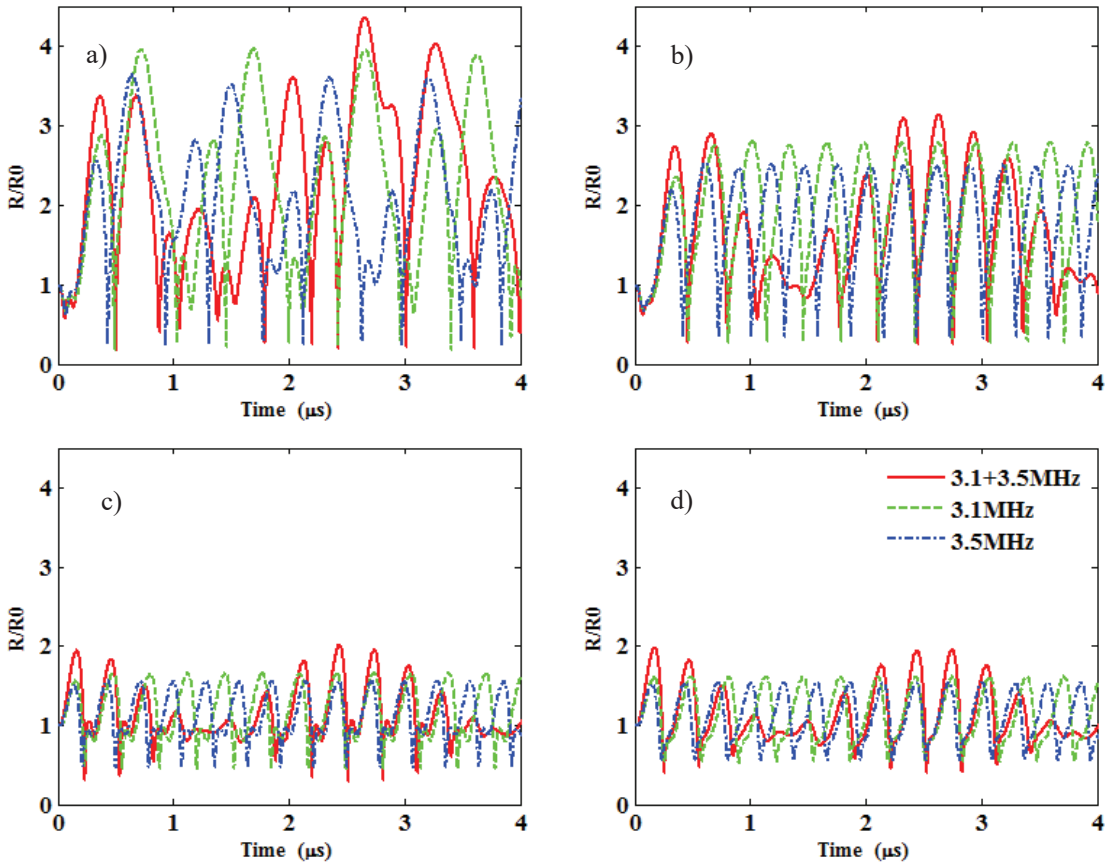

Figure 2

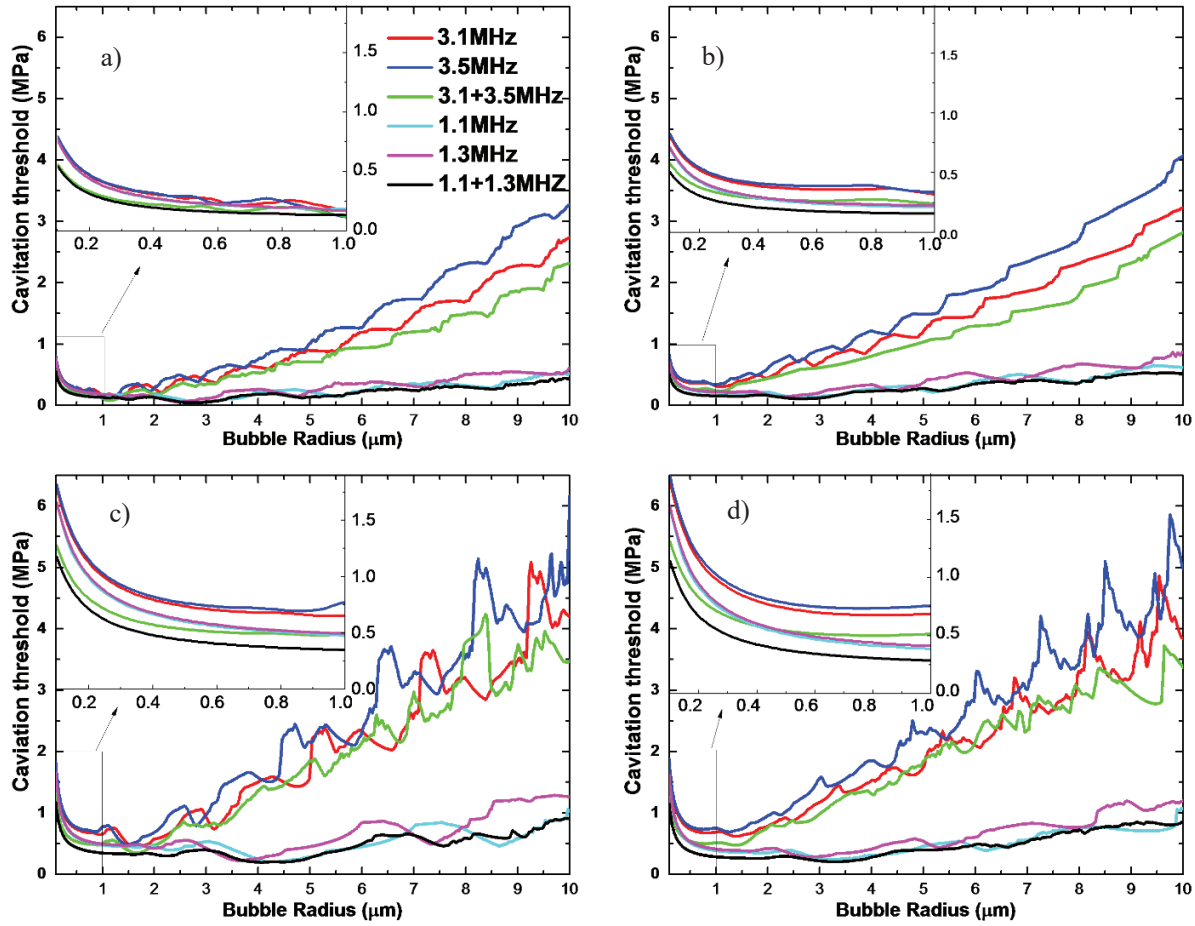
a)
b)
c)
d)
3.1MHz
3.5MHz
3.1+3.5MHz
1.1MHz
1.3MHz
1.1+1.3MHZ
Cavitation threshold (MPa)
Caviation threshold (MPa)
Bubble Radius (μm)

Figure 3

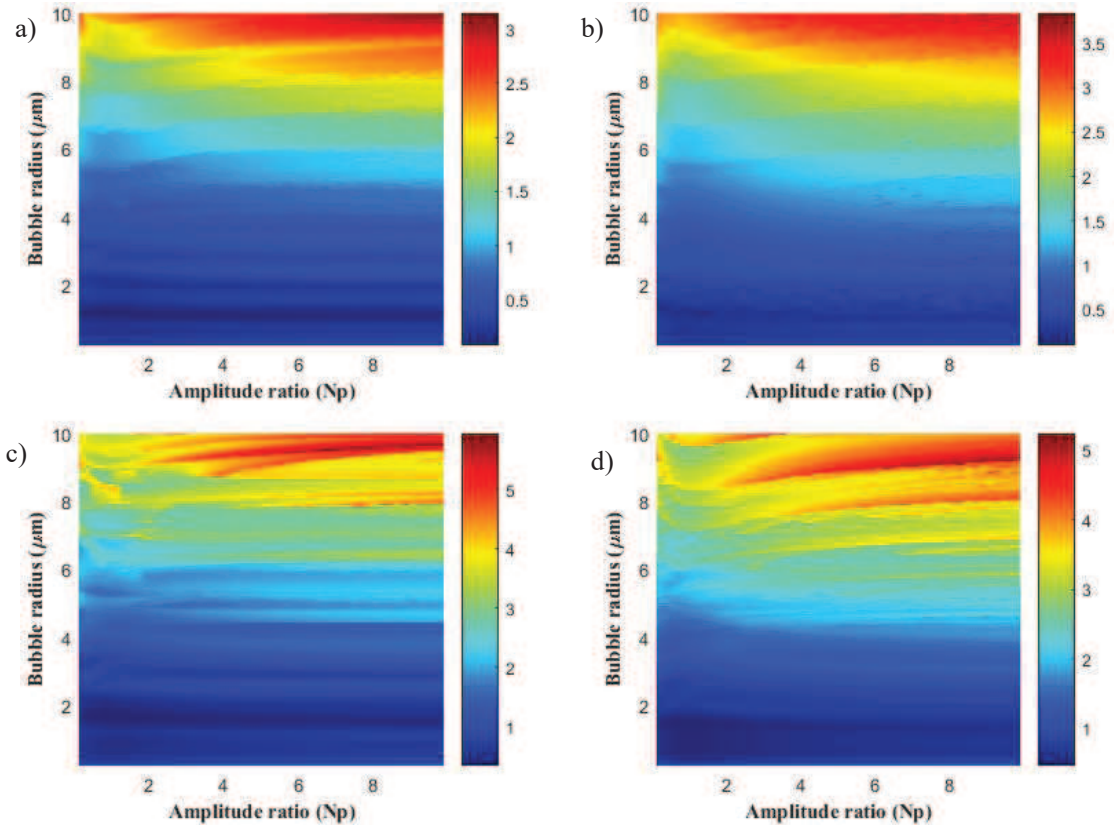

Figure 4

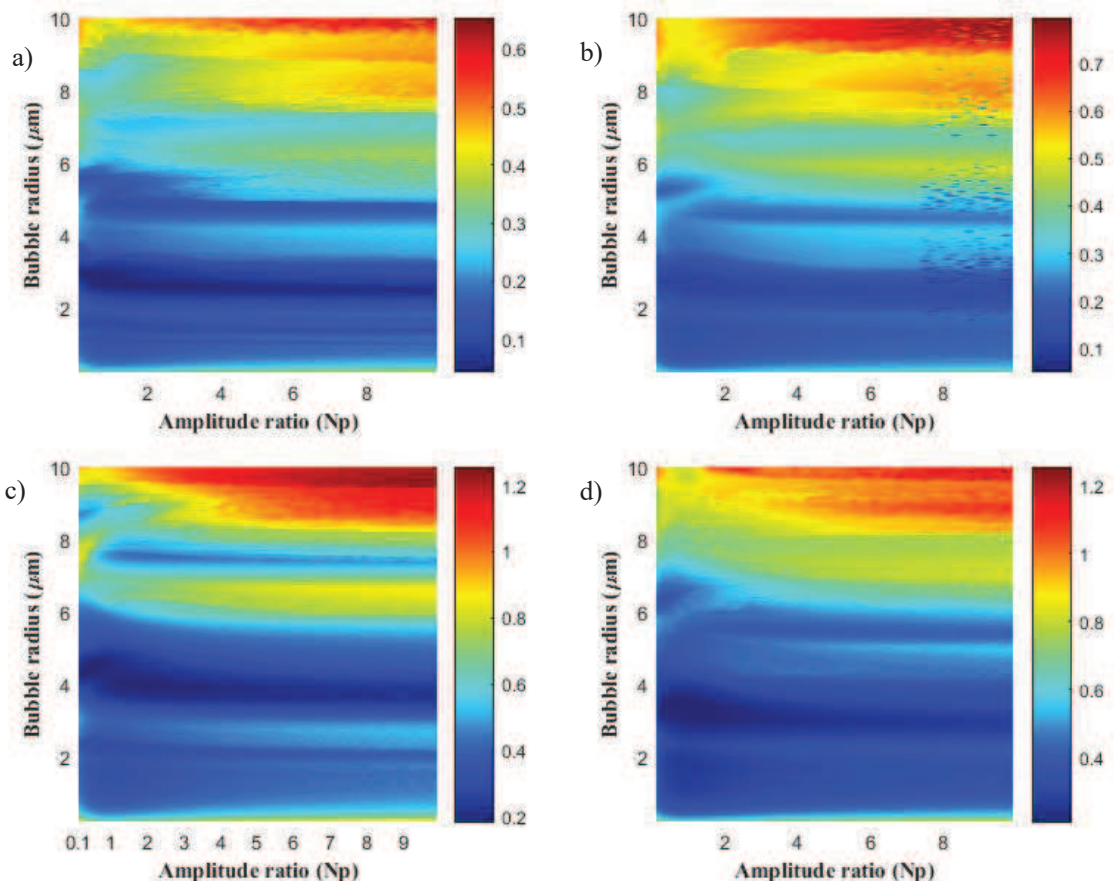

Figure 5

a)

b)

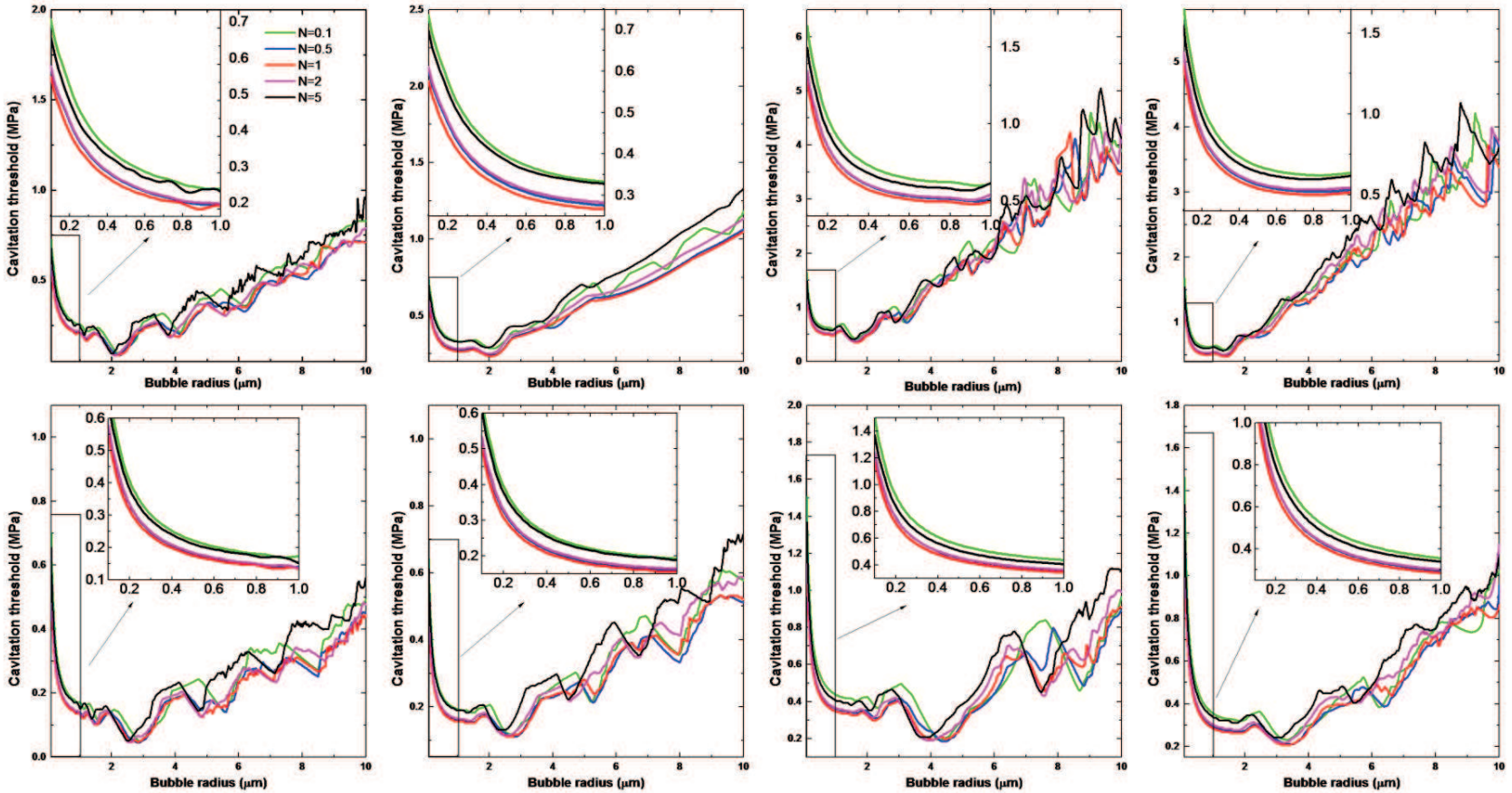

Figure 6

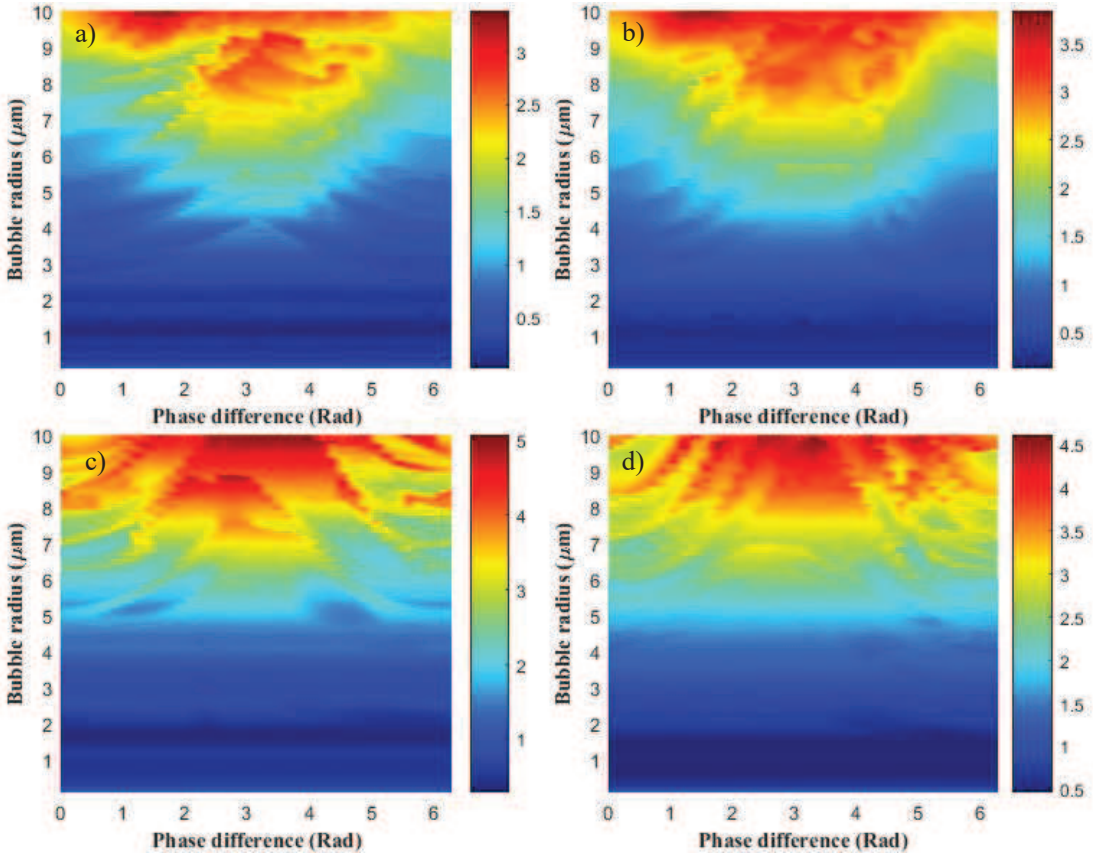

Figure 7

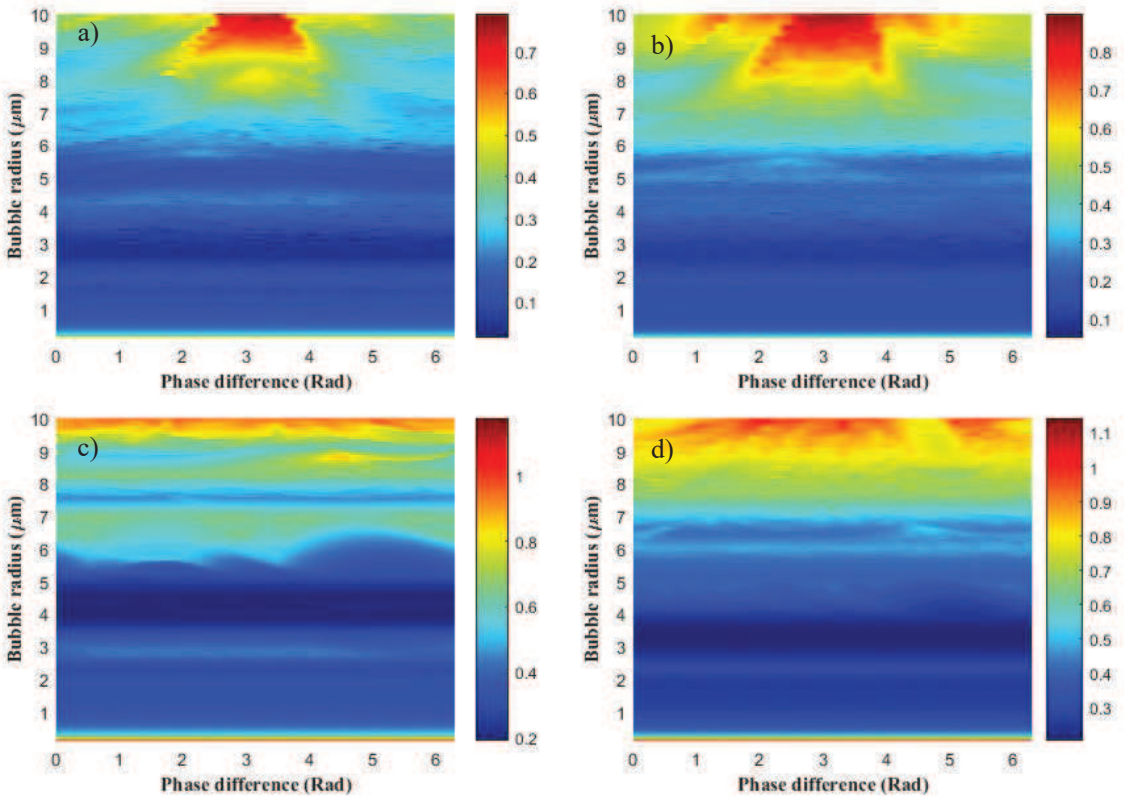

Figure 8

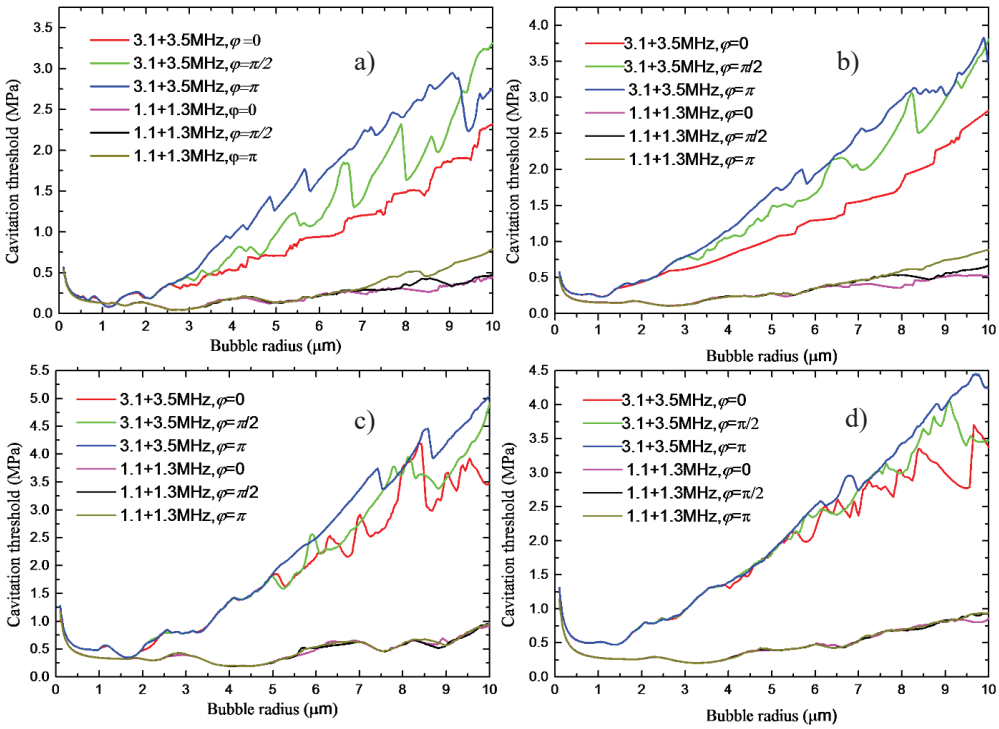
a)
3.1+3.5MHz,φ=0
3.1+3.5MHz,φ=π/2
3.1+3.5MHz,φ=π
1.1+1.3MHz,φ=0
1.1+1.3MHz,φ=π/2
1.1+1.3MHz,φ=π
Cavitation threshold (MPa)
Bubble radius (μm)
b)
3.1+3.5MHz,φ=0
3.1+3.5MHz,φ=π/2
3.1+3.5MHz,φ=π
1.1+1.3MHz,φ=0
1.1+1.3MHz,φ=π/2
1.1+1.3MHz,φ=π
Cavitation threshold (MPa)
Bubble radius (μm)
c)
3.1+3.5MHz,φ=0
3.1+3.5MHz,φ=π/2
3.1+3.5MHz,φ=π
1.1+1.3MHz,φ=0
1.1+1.3MHz,φ=π/2
1.1+1.3MHz,φ=π
Cavitation threshold (MPa)
Bubble radius (μm)
d)
3.1+3.5MHz,φ=0
3.1+3.5MHz,φ=π/2
3.1+3.5MHz,φ=π
1.1+1.3MHz,φ=0
1.1+1.3MHz,φ=π/2
1.1+1.3MHz,φ=π
Cavitation threshold (MPa)
Bubble radius (μm)

Figure 9

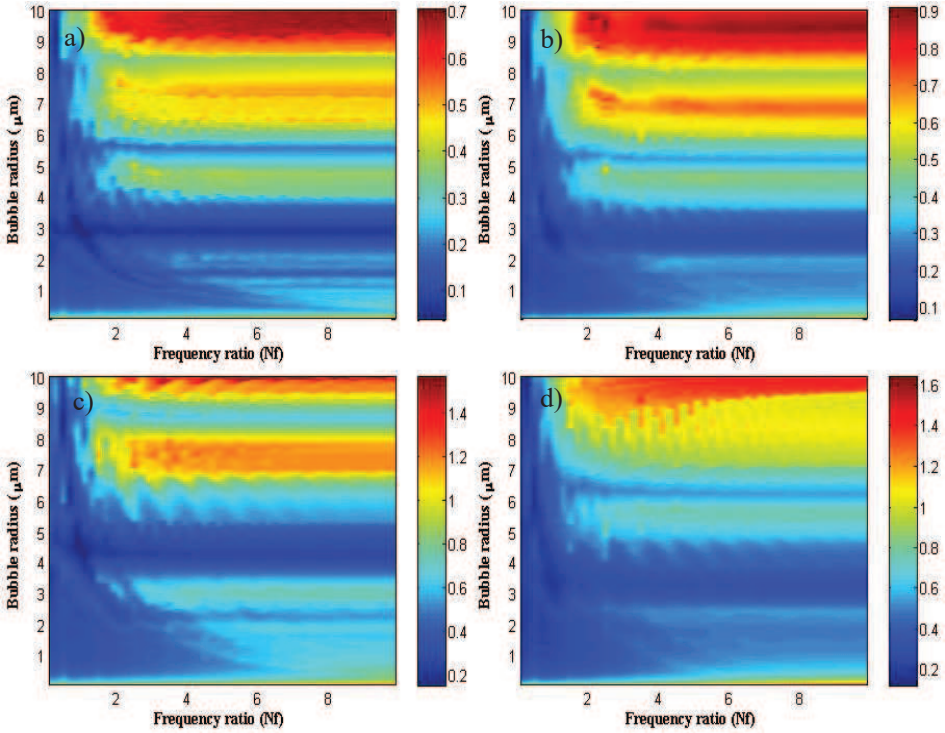

Figure 10

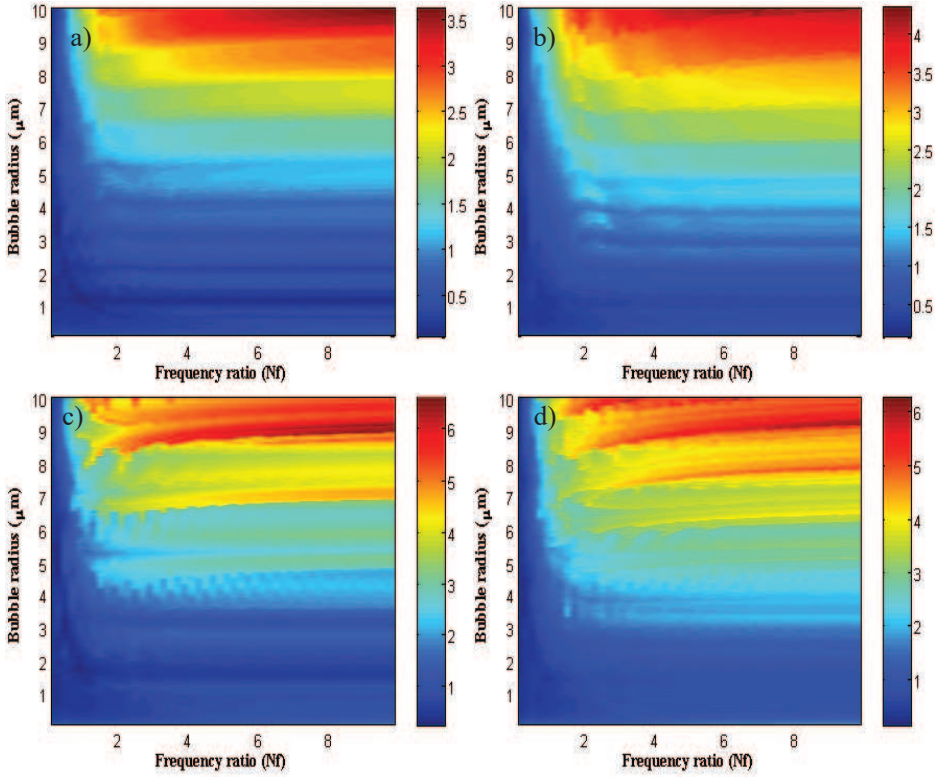

Figure 11

a)

b)

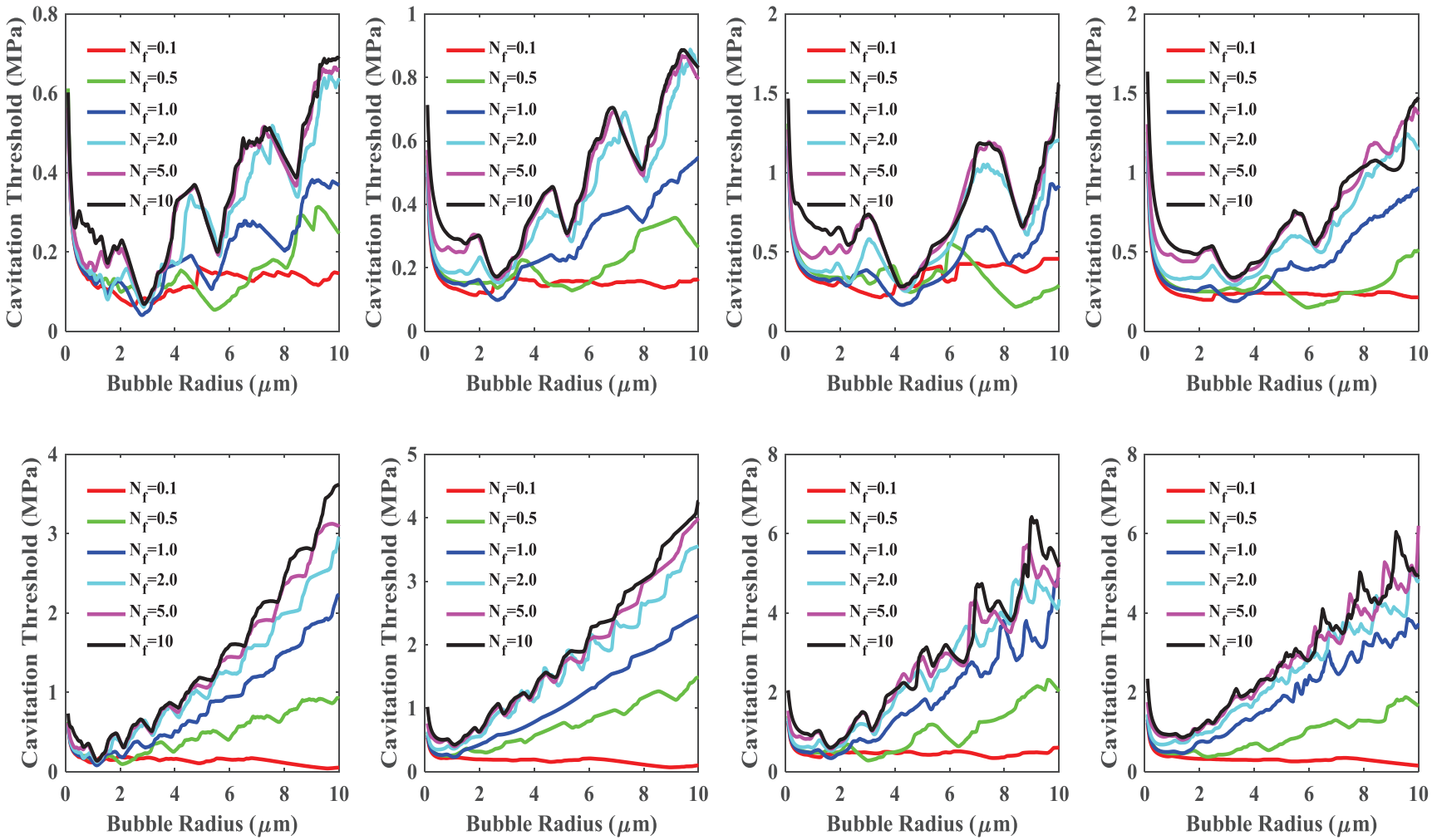
Cavitation Threshold (MPa)
Bubble Radius (μm)
N_f=0.1
N_f=0.5
N_f=1.0
N_f=2.0
N_f=5.0
N_f=10

Figure 12